Experimental Study of a Surface DBD Actuator Supplied by an Atypical Nanosecond Rising High-Voltage Pulse

Jérôme Pons, Hervé Rabat, Annie Leroy, and Dunpin Hong, *Member, IEEE*

***Abstract*— This paper presents experimental studies of a surface discharge of an aerodynamic actuator produced by a high-voltage pulse with a nanosecond rise time and a millisecond decrease time. Time-resolved imaging of the plasma and interferometric imaging of the shock wave generated by a unique nanosecond ramp were performed. Interferometry enabled shock fronts to be visualized with a 1 μs time resolution and to experimentally deduce for the first time the associated overpressure values. The interaction of the shock wave with the ionic wind generated during consecutive millisecond-scale voltage decay is also reported from phase-averaged laser Doppler velocimetry measurements. The observed phenomena were correlated with time-resolved images of the plasma developing at the dielectric surface during discharge phases.**

***Index Terms*— Ionic wind, nanosecond rise-time pulse, plasma actuator, shock wave, surface dielectric barrier discharge (SDBD).**

I. Introduction

TO FIND new devices capable of acting on flow to decrease vehicle energy consumption, our group, like many others, has experimentally studied different plasmas as airflow actuators [1]–[4]. For the past 15 years, surface dielectric barrier discharges (SDBDs) have been investigated as one of the main potential devices for subsonic flow control in aerodynamics [5], [6]. Until recently most reported work concerned sinus-driven SDBDs in the 1–10 kHz frequency range, corresponding to voltage rise-times in the millisecond (ms) range. For these discharges, the generation of an ionic wind is considered to be the main process governing plasma-to-flow interaction. The maximum velocity of the ionic wind is lower than 10 m/s [5], [6]. Although Kelley *et al.* [7] demonstrated, in a particular case, that such discharges can control high-speed flows, the potential applications of this actuator may be limited to low-speed external flows due to the slowness of the ionic wind. Consequently, in the past few years, there has been broadening interest in actuators using fast rise pulses in the nanosecond (ns) range, since this type of actuator may be used to control higher speed flows (up to 100 m/s) [8], [9]. Starikovskii *et al.* [8] demonstrated that the plasma interacts with the ambient medium by generating shock waves. The presence of the shock wave has been confirmed by numerical modeling [12].

In general, nanosecond discharges are produced by power supplies delivering almost square signals, consisting in two successive ns ramps, namely, positive and negative ramps, separated by a plateau of variable duration [2], [8]–[11]. For instance, in our previous work [2], the pulse width including rise and fall times was about 50 ns. These pulses were provided by a commercial pulsed high-voltage power supply (FID GmbH, FPG 20–50 KM).

In this paper, SDBDs were generated with a homemade power supply delivering a voltage pulse consisting in a nanosecond rise ramp (positive or negative) followed by millisecond range decay (negative or positive, respectively). This atypical power supply enables to observe the effect of a single ns ramp (positive alone, or negative alone).

To characterize the discharges, both voltage and discharge current were measured and the spatial and temporal evolution of the plasma structure was deduced from time-resolved imaging of the discharge using a gated intensified charge-coupled device (ICCD) camera. To observe the shock waves generated by the ns discharges, an imaging Mach–Zehnder interferometer was assembled. The advantage of this technique over other imaging techniques such as Schlieren visualization or shadowgraphy is that it enables convenient overpressure field value estimation. This is, to date, the first quantitative estimation of pressures in such waves. A time resolution of 1 μs was achieved, leading to evaluation of the wave propagation speed. Since the decay part of the pulse is in the ms range like kHz sinus-driven DBDs, an ionic wind is generated and was characterized using phase-averaged laser Doppler velocimetry (LDV). Velocity fields with a time resolution of about 5 μs were obtained, allowing for observation of the interaction between the ionic wind and shock waves in the vicinity of the discharge area.

This paper provides insight into the shock wave parameters, the ionic wind structures and their evolution induced by the discharges, and in particular, the differences

Manuscript received October 23, 2013; revised February 3, 2014; accepted April 22, 2014. Date of publication May 16, 2014; date of current version June 6, 2014. This work was supported by the 7th Framework Program EC FP7/2007-2013 through PLASMAERO under Grant 2342201.

J. Pons is with the Groupe de Recherches sur l'Energétique des Milieux Ionisés, Centre National de la Recherche Scientifique, University of Orléans, Orléans 45067, France, and also with the PRISME Laboratory, University of Orléans, Orléans 45072, France (e-mail: jerome.pons@univ-orleans.fr).

H. Rabat and D. Hong are with the Groupe de Recherches sur l'Energétique des Milieux Ionisés, Centre National de la Recherche Scientifique, University of Orléans, Orléans 45067, France (e-mail: herve.rabat@univ-orleans.fr; dunpin.hong@univ-orleans.fr).

A. Leroy is with the PRISME Laboratory, University of Orléans, Orléans 45072, France (e-mail: annie.leroy@univ-orleans.fr).

Color versions of one or more of the figures in this paper are available online at http://ieeexplore.ieee.org.

Digital Object Identifier 10.1109/TPS.2014.2321255

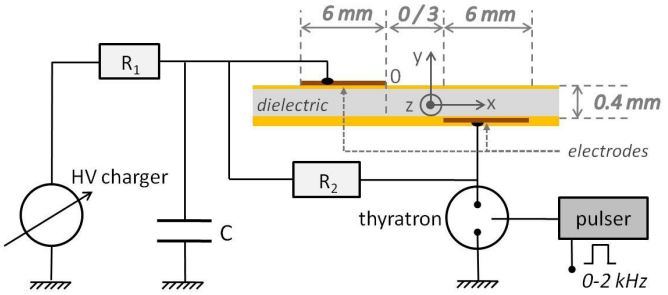

Fig. 1. Actuator (geometry, dimensions, and axes of the coordinate system for measurements) connected to the positive pulse-forming network.

between positive-slope and negative-slope discharges, either ns or ms.

II. Actuator Description and Electric Properties

Fig. 1 shows a schematic side view of the actuator and a representation of the electrical circuit providing the high-voltage pulse. The actuator consists of an asymmetric surface DBD, with parallel rectangular 100-mm-long, 6-mm-wide adhesive copper tape electrodes placed on each side of a dielectric. The gap distance between them is set at 0 or 3 mm. The dielectric is made of a 0.3-mm-thick polyethylene terephthalate sheet (Mylar variety) covered on both sides by two 0.05-mm-thick adhesive polyimide layers (Kapton HN variety or equivalent). This stack structure has a higher breakdown voltage than a single Mylar sheet. In addition, considering a stack structure with one Kapton layer and one Mylar layer, the discharge with Kapton in contact with plasma is similar to the one with Mylar in contact with plasma; but the first configuration allows a longer lifetime of the actuator. To prevent plasma formation on the bottom side, a dielectric layer (epoxy resin) was applied to the corresponding surface. The electrodes are referred to as active and inactive according to the possibility of forming plasma on their side or not. Fig. 1 also shows the x, y, and z coordinate system defined for imaging and LDV measurement analysis where the origin is placed at the edge of the active electrode, along its axis of symmetry.

The pulse-forming circuit consists of a capacitor ($C = 2$ nF), permanently charged by a HML 411 power supply (200 J/s capacitor charging unit) through a 47 kΩ resistor (R_1). The capacitor is also connected to the actuator grounded via a fast switch (Perkin-Elmer HY-3002 Thyratron). The voltage pulse is formed at the actuator poles when switch closure is triggered, causing the inactive electrode to reach ground potential and the voltage set across the capacitors to be transferred across the actuator within a ns-scale duration. The resulting voltage pulse obtained with a 15 kV charging voltage is shown in Fig. 2. Voltage is measured with a set of Tektronix P6015A probes (75 MHz bandwidth) placed at each pole of the actuator. The waveform shown in Fig. 2 results from subtraction of the two signals recorded with this set of probes. An enlargement of the rise part shows a 10%–90% rise time of around 30 ns, which is comparable with values found in the literature for similar experiments [8]–[11]. Thyratron closing

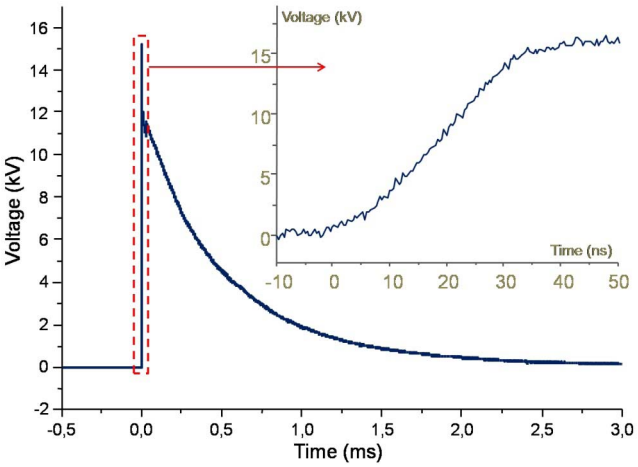

Fig. 2. Voltage pulse (15 kV), full view and enlargement of the ns rise.

triggered by a pulse generator at an adjustable frequency (0–2 kHz) takes place for about 1 μs, leading to a plateau during which the voltage maintains a constant value (as shown by the inset in Fig. 2). After switch reopening, the resistor R_2 connected parallel to the actuator causes the voltage to return to zero, resulting in the exponential decay observed on the voltage pulse. R_2 is inactive during switch closure because of its high resistance value (typically $R_2 = 15$ MΩ, adjusted with the working frequency). The characteristic time of this exponential decay, in the conditions shown in Fig. 2, is close to 0.5 ms. The pulse can be generated in single shot or repetitive mode at a frequency up to 2 kHz.

To identify the active phases of such a pulse, the discharge current was measured using a Bergoz CT-C1.0-B (500 MHz bandwidth, 1 V/A sensitivity) probe placed around the wire connecting the actuator to the Thyratron. The result for a no-gap actuator is shown in Fig. 3. A strong current pulse with a 27 A magnitude is obtained during the ns rise with a 15 kV charging voltage. Pulse duration (full width at 10% of the maximum) is close to 30 ns. Different shots at this voltage systematically lead to a similar pulse, with marginal variations (±1 A). For power estimation, the current pulse can be approximated by a triangle with a 30 ns base duration and a 27 A peak value. Since the voltage increases almost linearly from 0 to 15 kV, the total dissipated energy during this ns pulse can be calculated analytically and is close to 3 mJ. The mean power during the 30 ns is thus about 100 kW.

During voltage decay, a set of negative pulses with much lower intensity (absolute value in the 0.1–1 mA range, therefore with different scaling from ns pulse range) can be detected after the voltage has decreased to below half its initial value (not shown here). Different shots lead to similar statistical properties of these pulses, but not systematically to the same pulses at the same time and with similar intensities. Therefore, the ms decay leads to a discharge with similar characteristics to those of the negative half-cycle of a kHz sinus-driven DBD. Generation of such discharge is due to positive charge deposition at the dielectric surface following ns positive rise pulse, causing a positive

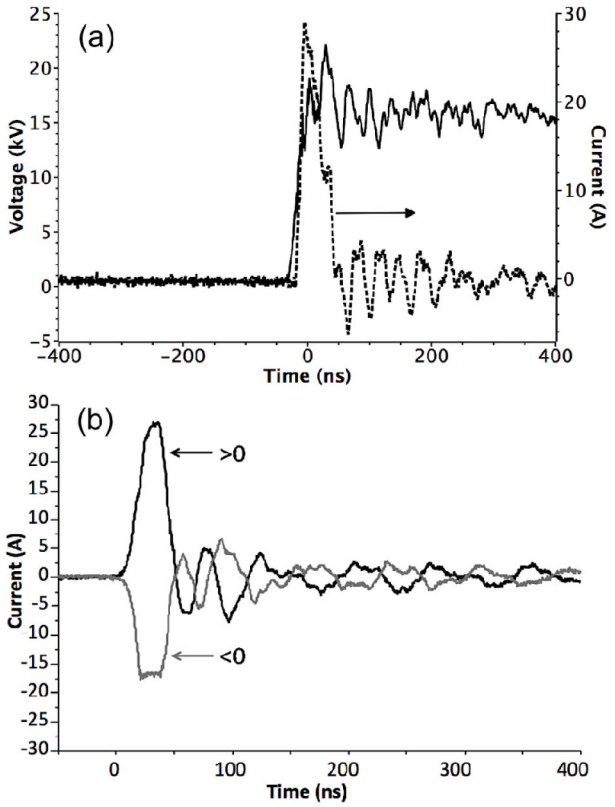

Fig. 3. (a) Nanosecond current pulse at ±15 kV with no-gap actuator. (b) Positive ns pulse superimposed to the voltage pulse.

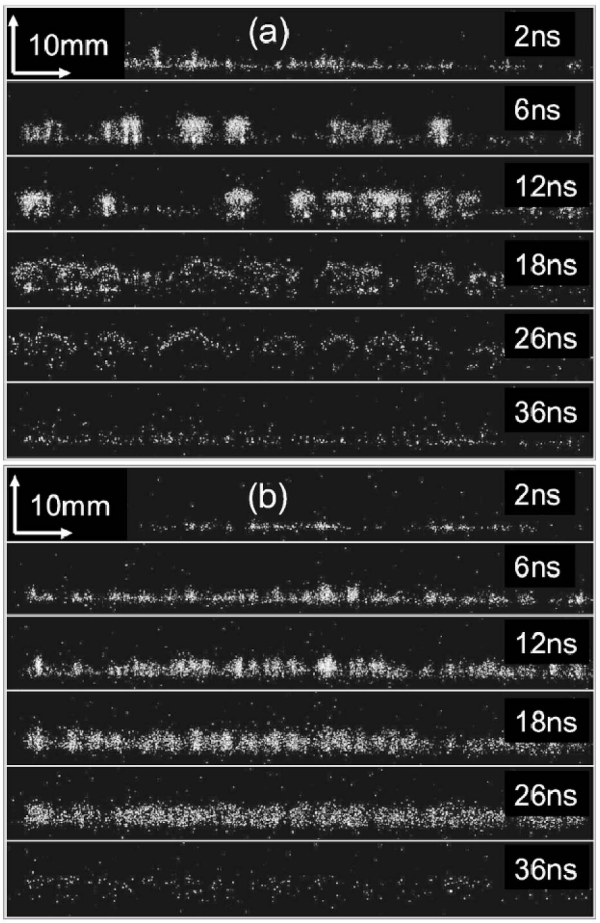

Fig. 4. Plasma evolution during ns discharge, illustrated with a set of six pictures each at (a) 15 kV and (b) −15 kV, for 1 kHz repetition rate (exposure time = 2 ns).

electric potential; when the difference with the electrode potential decreases below the breakdown threshold such ms pulses appear.

To investigate the effect of discharge polarity, one should apply to the actuator the same pulse as that shown in Fig. 2 but with the opposite sign; connections to the circuit were reversed (active electrode connected to the Thyratron, and inactive electrode to the capacitor). The reversed pulse thus obtained is further referred to as negative. As shown in Fig. 3, a −15 kV pulse results in a main pulse with similar features to those in positive regime, except for its magnitude (−17 A) which is about one third lower. This means that a negative pulse leads to a less energetic discharge, in agreement with recently published work on similar devices [10]. During voltage decay stochastic pulses were detected in a similar way, but were observed to be more intense than the previous ones (in the 10–100 mA range, with different scaling from ns pulse range). Again these characteristics are comparable with those measured for positive half-cycles of sinus-driven DBDs. The same interpretation as above can be made, for reverse polarities.

The measured pulses shown in Fig. 3 in fact correspond to the superimposition of the displacement current (related to the capacitive nature of the DBD) and the component deriving from plasma formation at the actuator surface. An estimation of the actuator equivalent capacitance gave a value of 3 pF, which results in a displacement current with a peak value around 1 A (15 kV, 30 ns pulse). Considering the total measured current the displacement current can be considered negligible with the above operating conditions.

The following reported results all correspond to ±15 kV pulses applied to 0 or 3 mm gap actuators. The current properties for 3 mm gap actuators are more or less similar to those shown in this section for 0 mm gap actuators.

III. Plasma Imaging

The evolution of the plasma structure during the ns discharge was observed using time-resolved imaging with an intensified gated CCD camera (Andor iStar) mounted with an objective lens for observation in the visible range. Considering the voltage rise time in these experiments, a 2 ns duration for the gate width of the CCD was chosen as the time resolution. Images were taken in the (x, z) plane (see Fig. 1).

The plasma evolutions of positive and negative ns discharges are shown in Fig. 4 for a 0 mm gap actuator under a ±15 kV pulse at 1 kHz (the active electrode is below the emissive area). For both polarities, the plasma consists in several filaments distributed on the dielectric surface, ignited collectively along the electrode tip and propagating toward the dielectric. Positive filaments present branched structures that extend 8-mm away from the electrode, whereas negative filaments are straight

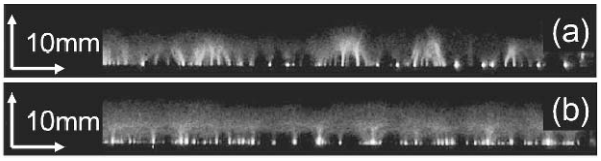

Fig. 5. Time-integrated (exposure time = 0.6 ms) plasma during ms voltage decay after (a) 15 kV ns discharge or (b) −15 kV ns discharge. Remember that a +15 kV ns discharge is followed by a −15 kV ms discharge. Therefore the picture at the bottom corresponds to a 15 KV ms discharge, while the photo at the top corresponds to a −15 kV ms discharge.

and extend only 5-mm away. Such collective behavior is consistent with the unique intense current pulse measured: the formation of multiple channels releases a large amount of charges, whereas a single filament would lead to pulses such as those detected during the ms decay. At the end of the ns positive discharge, the filaments separate into two parts: one attached to the electrode and the other onto the dielectric surface as illustrated by pictures taken at the moment 18, 26, and 36 ns (Fig. 4). This marks the end of charge transfer through these channels and therefore the end of the discharge.

The plasma was observed with a similar technique during the ms voltage decay, with a longer integrating time, for both polarities. Images integrated over most of the ms decay are shown in Fig. 5 for both polarities. The plasma structures observed are very similar to those of the ns discharge. Filament lengths are about the same for the equivalent polarities, suggesting that the extension lengths are independent of the voltage rise time but are intrinsic to the polarity, for a given absolute voltage value. In other words in the present conditions, positive filaments extend 8-mm away from the electrode tip, and negative filaments extend 5-mm away from the electrode tip. The major difference between ns and ms discharges concerns filament ignition: in ms discharges it is individual instead of collective, with one current pulse corresponding to a single filament. Unlike the filament length this property depends only on the rise time but not on the polarity. It has indeed been confirmed by recent observations, with sinus-driven DBDs in either the kHz or MHz range [13], [14]. In the latter case, voltage rise times are comparable to the ns regime, and collective breakdown has been experimentally evidenced [10]. In the kHz range, except for a unique set of experiments involving specific conditions [15], no other collective breakdown has been reported to date, especially with actuators similar to those used in this paper.

IV. Shock Wave Observation and Characterization

A. Experimental Setup

The intense current pulse resulting from an ns voltage rise is likely to induce fast heating of the air undergoing ionization in the plasma channels and to result in the generation of a thermal shock wave as an energy release process, according to the physical interpretation of Starikovskii *et al.* [8]. To observe and quantitatively characterize these waves, a Mach–Zehnder interferometer coupled with a fast ICCD camera (Andor iStar) or a CMOS camera (Photron Fastcam SA5 1000K-M2) was

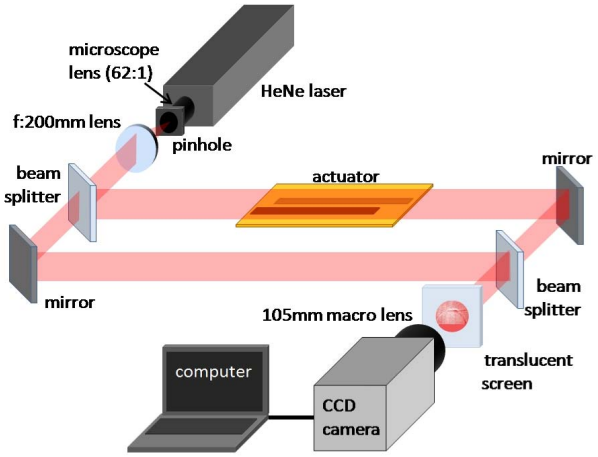

Fig. 6. Interferometer setup.

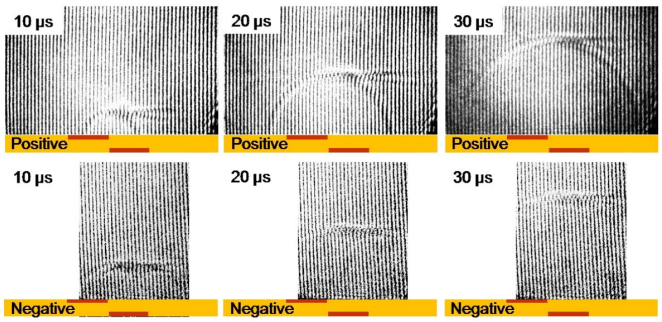

Fig. 7. Shock wave propagation following ±15 kV ns pulses above 0 mm gap actuators (1 μs exposure time).

set up (see Fig. 6). The expanded beam of a 632.8 nm He–Ne laser (15 mW) was used to produce parallel fringes of equal thickness on a translucent screen at the apparatus outlet. The fringes were arranged orthogonally to the actuator surface. The CCD was used to acquire the interference figure displayed on the screen. When the shock wave is generated, the consecutive compression or expansion of the air inside the wave front results in refraction index modifications, which appear in the interference figure as fringe distortions. By measuring fringe shifts, it is therefore possible to deduce the related index variations, and thus an estimation of the local related overpressure can be obtained using classical gas laws.

B. Shock Wave Images

Images were taken with 0-mm gap actuators excited with a ±15 kV pulse, in single mode with a minimum time lapse of 1 min between two consecutive shots, to allow for sufficient surface cooling. Fig. 7 shows interference figures perturbed by shock waves induced by positive and negative pulses, at different times following discharge onset (from 10 to 30 μs), and with a time resolution of 1 μs (the position of the electrodes is shown on each picture). At times below 7 μs, the wave is too close to the surface to be observable with a chance for being processed, which explains the chosen time frame. These images are in the (x, y) plane as shown in Fig. 1.

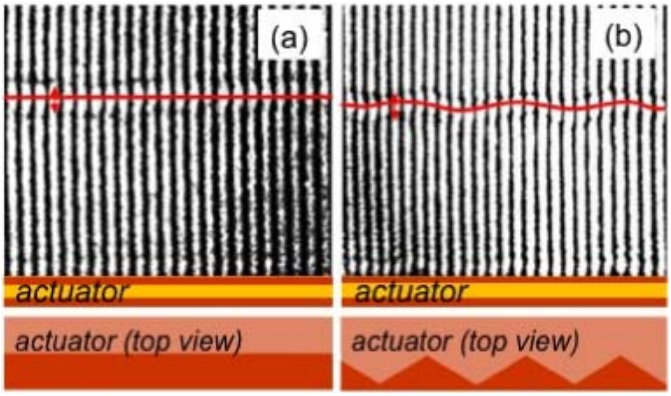

Fig. 8. Shock wave at $t = 20$ μs in the (y, z) plane induced by a 15 kV pulse for a 0 mm gap actuator and for 1 μs of exposure time. (a) Straight electrode. (b) Sawtooth electrode.

For positive pulses the images were recorded with the Andor iStar camera, whereas for negative pulses requiring a better contrast they were recorded with the Photron camera. The differences in image widths are due to the different frame dimensions with the two cameras. Horizontal scale is given by the electrode width, which equals 6 mm; vertical scale is similar.

It reveals that the perturbed zone appears as the superimposition of two parts: a circular part, centered at the active electrode edge along the z-axis, and a quasi-rectilinear part parallel to the dielectric surface in the x-axis, extending above the plasma area and tangential to the circular part. The perturbation appears similar to both discharge polarities, although the circular part is less visible with the negative discharge, which may point to a weaker shock wave. This shape is in agreement with images captured with similar discharges previously reported [8]–[10].

The propagation speeds deduced from these measurements are around 600 m/s at the earliest instants, and decrease rapidly to stabilize around 400 ± 50 m/s for $t > 40$ μs. The speed is the ratio of wave position shifts on two successive images to the corresponding elapsed time between the images, and its uncertainty was estimated to be close to 50 m/s. For the present conditions, the speeds for negative and positive polarities were found to be very close to each other for a given time. One can notice that the speed values are slightly higher than those found in literature (see for instance [8]), but in the same range.

To better interpret the 3-D shape of the shock wave, interference figures were captured with the discharge rotated through 90° (longitudinal side view), leading to images in the (y, z) plane (see Fig. 1). Fig. 8(a) shows one of these figures, and the perturbation on the fringes appears almost perfectly rectilinear above the plasma area. Correlation with the (x, y) view shows that it corresponds to the top of the circular part extended by the rectilinear part. The fact that the circular part does not appear can be explained by the superimposition of shock waves induced by all the discharges and shows quasi uniformity of streamer distribution at the actuator surface. Confirmation of this fact was obtained using sawtooth electrode geometry [4] [Fig. 8(b)]: at the tip of every sawtooth, where intense streamers are formed, a circular wave appears. The rectilinear wave observed on Fig. 8(a) can be interpreted as the sum of the circular waves produced by all the streamers generated simultaneously as shown by ICCD imaging (see Section III). It can therefore be concluded that the shock wave has a cylindrical shape with the electrode edge (z-axis) as its main axis, and tangentially extended by a quasi-planar part parallel to the surface.

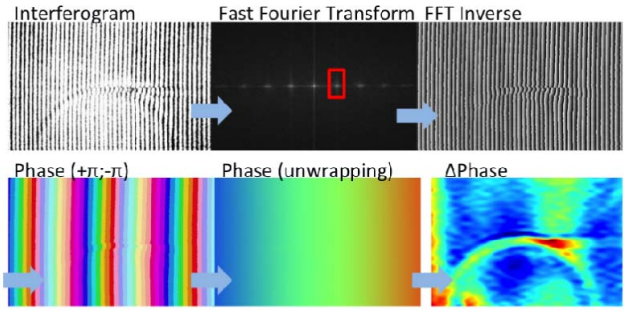

Fig. 9. Interferogram processing steps (rectangle in the FFT figure illustrates band-pass filtering).

C. Quantitative Analysis and Comparison with Simulations

To quantitatively analyze these observations, the images were processed as follows: raw data (2-D matrices with measured intensity gray levels) were filtered using band-pass filter on their fast Fourier transform (FFT) for noise reduction and contrast enhancing. Conversion to wrapped phase (varying between $-\pi$ and π) in first place, and then to unwrapped phase (varying from 0 to infinity) leads to the phase map, which after subtraction to an unperturbed image, yields the phase shift mapping of the interferogram. These steps are shown in Fig. 9, and more details can be found in [16].

From the phase shift $\Delta\varphi$, the refractive index variation Δn was deduced with the following relation:

$$\Delta n = n - n_0 = \Delta\varphi \times \frac{\lambda}{2\pi L}$$

where n and n_0 are the refractive indices of perturbed and unperturbed air respectively, λ the laser wavelength and L the perturbation length. To use this equation, it is assumed that the perturbation is independent of the coordinate orthogonal to the image plane (2-D assumption). Tests with various electrode lengths showed that in the present conditions this assumption is reasonable for images in the (x, y) plane. For an ideal gas, the pressure p is related to the refractive index by the Gladstone–Dale equation

$$n = 1 + \frac{pK}{RT}$$

where K is the Gladstone–Dale constant of the air at the laser wavelength, R is the ideal gas constant, and T is the gas temperature. The latter is assumed to be constant and uniform, which is reasonable if dielectric heating consecutive to discharge running can be neglected. According to thermographic measurements previously reported for surface DBDs [17], and considering the fact that the discharge used here is run in single shot mode, heating can be considered negligible. These facts

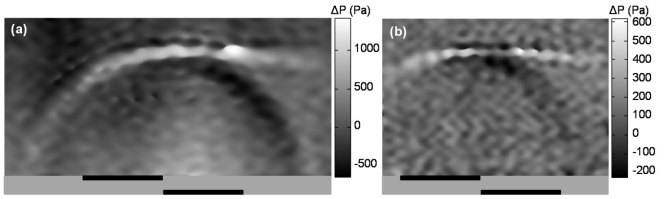

Fig. 10. Experimental pressure levels of the shock wave for (a) 15 kV and (b) −15 kV pulses at $t = 20$ μs and for 0 mm gap actuator.

are corroborated by energy and temperature calculations from discharge modeling [11]. Finally, pressure variation can be deduced from phase shift by the following relation:

$$\Delta p = p_0 \times \frac{\Delta\varphi \times \lambda}{(n_0 - 1) \times 2\pi L}$$

where p_0 = atmospheric static pressure (10^5 Pa). Compared with classical shock wave visualization techniques such as shadowgraphy or Schlieren visualization, this method has the advantage of leading quite easily to the associated quantitative values.

Using this processing technique, the overpressure (further referred to simply as pressure) fields were deduced from these images. Results with a 0-mm gap actuator for the two polarities at $t = 20$ μs are shown in Fig. 10. It shows a pressure excess (positive pressure) on one half of the circular part and on the planar part, and a pressure deficit (negative pressure) on the second half of the circular part, situated above the plasma. The maximum pressure is obtained at the junction of the cylindrical and planar parts. In the present conditions, it is estimated to be about 1500 Pa with a positive pulse and 600 Pa with a negative pulse. The minimum is about −600 Pa for positive pulses, and −200 for negative pulses. In consistency with their lower peak current, it confirms that negative discharges transfer a lower amount of energy to the shock wave. The negative-to-positive ratio of maximum over pressures is close to 40%, lower than the one found for current values (about 63%). However, owing to the lower resolution achieved with the Photron camera, the value for the negative discharge is clearly underestimated (peak values are smoothed during image processing). According to the relative uncertainty on the measurement of phase shift, the relative uncertainty on the determination of the overpressure is estimated at 30%. Therefore, the accuracy on overpressure values is around ±450 Pa for positive discharges (Andor camera) and ±180 Pa for negative discharges (Photron camera). Considering these uncertainties, the result is consistent with the one found for current values.

Results for 3-mm gap actuators in similar conditions lead to similar results, with comparable pressure ranges (Fig. 11). With positive discharges, the wave is slightly less intense (1400 Pa), whereas with negative discharges it appears to be twice as high (1200 Pa). The negative-to-positive ratio found here is higher than 80%. Both images were taken with the Andor camera, therefore uncertainties are, respectively, ±420 Pa and ±360 Pa. Again with this range of values the result is consistent with current measurements. The circular

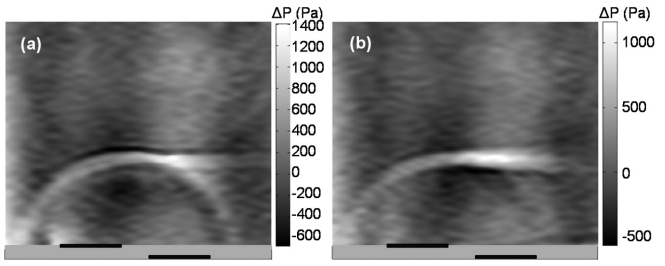

Fig. 11. Experimental pressure levels of shock wave for (a) 15 kV and (b) −15 kV pulses at $t = 20$ μs for 3 mm gap actuator.

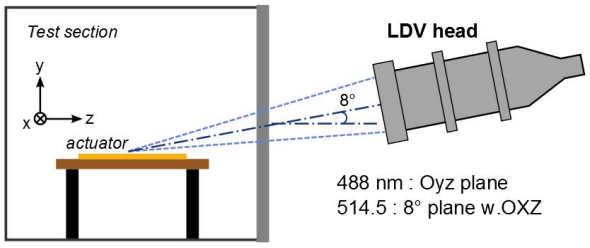

Fig. 12. LDV apparatus.

part of the wave corresponds here to both positive and negative pressures above the plasma. With negative discharges, the negative pressure part even almost disappears.

V. Ionic Wind Velocity Measurement and Interaction With the Shock Wave

The ionic wind velocity generated during the ms part of the pulse was measured at different points above the dielectric surface, with a two-component LDV system (Dantec Dynamics BSA 51N) using the 488 and 514.5 nm beams of an ionized Ar laser. The actuator was placed in a closed chamber at atmospheric pressure, and measurement was performed in initially motionless air seeded with oil droplets (see Fig. 12). This system is similar to the devices used in characterizing the ionic wind generated by sinus-driven DBDs [18], [19]. A 3-mm gap discharge operating in repetitive mode at 1 kHz and ±15 kV was used. The velocity components u and v, respectively, along the x and y axes were deduced from phase averaging over a 120 s acquisition with a 0.5–1 kHz acquisition rate. The velocity modulus U and tilt angle θ (defined by the angle between velocity vector and x-axis) are calculated from u and v using the following definitions:

$$U = \left(u^2 + v^2\right)^{1/2} \quad \tan\theta = v/u.$$

A time resolution of about 5 μs was achieved with these operating conditions. The acquisition frame was set every 2 mm from $x = 1$ to 11 mm along the horizontal direction, and every 0.1 mm from $y = 0.1$ to 0.9 mm, every 0.3 mm up to $y = 1.5$ mm and every 0.5 mm up to $y = 3$ mm along the vertical direction. The discharge circuit and LDV acquisition system are synchronized by the same signal, and the time scale starts at the onset of the ns discharge as shown in Fig. 2.

Fig. 13 shows the time evolution of U and θ over a period at two locations: a fixed point (further mentioned as point A)

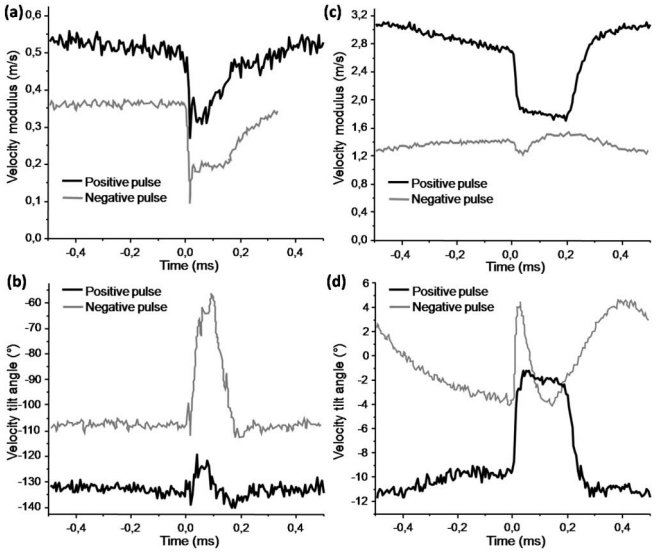

Fig. 13. Temporal variations of U (modulus) and θ (angle) over a 1 ms period at (a) and (b) point A and at (c) and (d) point B.

above the dielectric surface, almost vertical to the active electrode edge ($x = 1$ mm, $y = 3$ mm), and a point where the average velocity was maximum (further mentioned as point B), thus depending on the polarity. In the above conditions, this point is at $x = 5$ mm, $y = 0.7$ mm when the ns pulse is positive, and $x = 9$ mm and $y = 0.5$ mm when the ns pulse is negative. These positions correspond to the extension lengths of the plasma filaments observed during the voltage decay phase by time-resolved imaging.

At point A, the flow velocity U is between 0.3 and 0.55 m/s with a positive pulse, and between 0.15 and 0.35 m/s with a negative pulse. Four phases can be observed in its evolution: at $t = 0$ a sharp deceleration, followed by a lapse of time during which no variation occurs, then gradual acceleration to the maximum value, and finally another constant velocity period of time. Two active phases can therefore be highlighted: the acceleration and deceleration phases, occurring, respectively, during the ms and ns discharges, simultaneously to the appearance of plasma at the actuator surface. Deceleration occurs about 5–10 μs after the ns discharge, which includes the time for the shock wave to reach point A considering the measured wave speed. A likely explanation for this deceleration therefore may be the shock wave which induces probably a strong depression at point A. The acceleration process is certainly similar to the ionic wind measured with ac actuators [18], [19]. Indeed, it is shown here that positive-going voltage (with negative pulse) generates a lower velocity than negative-going voltage (with positive pulse). At point A, the velocity vector is oriented almost vertically toward the electrode tip, with θ angles during the still phases close to $-110°$ (negative pulse) or $-130°$ (positive pulse). The deceleration corresponds to an increase in the angle. With a positive pulse, θ returns to its initial value during acceleration, whereas with a negative pulse, this phenomenon seems to occur slightly earlier.

At point B similar behaviors are observed with the positive pulse. The only notable difference is with the still phases, during which flow deceleration is more marked than at point A. This could be due to the closer proximity of the surface, where viscosity effects might be enhanced. With a negative pulse a dramatically different behavior is observed: relatively small velocity variations are observed, and acceleration takes place almost immediately after the ns discharge. θ undergoes an increase during the active ms discharge phase (i.e., the period of time during which plasma is observed). As at point A, the negative-going ms voltage induces a higher velocity than the positive-going velocity (twice as high at the present voltage). However, at point B the velocity vector is directed almost tangentially to the actuator surface, with θ close to 0 (negative pulse) or $-10°$ (positive pulse). Considering the orientations measured at these points, and also on the whole measurement grid, the flow appears to have the same features as a wall jet. This is similar to the results found with sinus-driven DBDs [18], [19].

VI. Conclusion

The effects of positive and negative nanosecond pulsed DBD actuators have been investigated, applying a pulse combining a 30-ns ramp and a ms-scale decay. The time-resolved imaging reveals two plasmas that are different in shape and in length for positive and negative ramps and a collective ignition of discharges all along the active electrode for the ns ramps, compared with inhomogeneous plasma for the ms ramps. Shock wave fronts detected by time-resolved imaging interferometry have been found to propagate at speeds of around 400 m/s. The associated overpressure fields deduced from these images show that the wave cylindrical part corresponds to a pressure excess on one half and a pressure deficit on the other half, whereas the planar part tangentially connected to it corresponds to a pressure excess. The pressure in the shock wave ranges from -600 to 1500 Pa, 20 μs after the discharge. Higher-energy waves are generated with a positive ns pulse, which agrees with the higher current pulse measured simultaneously. The interaction with the ionic wind generated during the ms part, characterized using time-resolved LDV, shows the sudden change in the flow consecutive to the shock wave. Furthermore, the properties of the ionic wind generated during the ms decay correspond to those of sinus-driven DBDs.

References

[1] P. Magnier, D. Hong, A. Leroy-Chesneau, J. M. Bauchire, and J. Hureau, "Control of separated flows with the ionic wind generated by a DC corona discharge," *Experim. Fluids*, vol. 42, no. 5, pp. 815–825, 2007.

[2] P. Magnier, B. Dong, D. Hong, and J. Hureau, "Action of a pulsed DBD actuator on a slow jet," *J. Electrostatics*, vol. 66, no. 7, pp. 369–374, 2008.

[3] B. Dong, D. Hong, J. Bauchire, and J. Pouvesle, "Experimental study of a gas jet generated by an atmospheric microcavity discharge," *IEEE Trans. Plasma Sci.*, vol. 40, no. 11, pp. 2817–2821, Nov. 2012.

[4] R. Joussot, A. Leroy, R. Weber, H. Rabat, S. Loyer, and D. Hong, "Plasma morphology and induced airflow characterization of a DBD actuator with serrated electrode," *J. Phys. D, Appl. Phys.*, vol. 46, no. 12, p. 125204, 2013.

[5] E. Moreau, "Airflow control by non-thermal plasma actuators," *J. Phys. D, Appl. Phys.*, vol. 40, no. 3, pp. 605–636, 2007.

[6] T. C. Corke, M. L. Post, and D. M. Orlov, "Single dielectric barrier discharge plasma enhanced aerodynamics: Physics, modeling and applications," *Experim. Fluids*, vol. 46, no. 1, pp. 1–26, Jan. 2009.

[7] C. L. Kelley, P. Bowles, J. Cooney, C. He, and T. C. Corke, "High Mach number leading-edge flow separation control using AC DBD plasma actuators," in *Proc. 50th AIAA Aerosp. Sci. Meeting*, Nashville, TN, USA, Jan. 2012.
[8] A. Y. Starikovskii, A. A. Nikipelov, M. M. Nudnova, and D. V. Roupassov, "SDBD plasma actuator with nanosecond pulse-periodic discharge," *Plasma Sources Sci. Technol.*, vol. 18, no. 3, p. 034015, 2009.
[9] M. Nishihara, K. Takashima, J. W. Rich, and I. V. Adamovitch, "Mach 5 bow shock control by a nanosecond pulse surface dielectric barrier discharge," *Phys. Fluids*, vol. 23, no. 6, pp. 066101-1–066101-11, 2011.
[10] N. Benard, N. Zouzou, A. Claverie, J. Sotton, and E. Moreau, "Optical visualization and electrical characterization of fast-rising pulsed dielectric barrier discharge for airflow control applications," *J. Appl. Phys.*, vol. 111, no. 3, p. 033303, 2012.
[11] K. Takashima, Z. Yin, and I. V. Adamovich, "Measurements and kinetic modeling of energy coupling in volume and surface nanosecond pulse discharges," *Plasma Sources Sci. Technol.*, vol. 22, no. 1, p. 015013, 2013.
[12] T. Unfer and J. P. Boeuf, "Modelling of a nanosecond surface discharge actuator," *J. Phys. D, Appl. Phys.*, vol. 42, no. 19, p. 194017, 2009.
[13] P. Audier, R. Joussot, H. Rabat, D. Hong, and A. Leroy, "ICCD imaging of plasma filament in a circular surface dielectric barrier discharge arrangement," *IEEE Trans. Plasma Sci.*, vol. 39, no. 11, pp. 2180–2181, Nov. 2011.
[14] J. Dedrick, R. W. Boswell, P. Audier, H. Rabat, D. Hong, and C. Charles, "Plasma propagation of a 13.56 MHz asymmetric surface barrier discharge in atmospheric pressure air," *J. Phys. D, Appl. Phys.*, vol. 44, no. 20, p. 205202, 2011.
[15] K. Allegraud, O. Guaitella, and A. Rousseau, "Spatio-temporal breakdown in surface DBDs: Evidence of collective effect," *J. Phys. D, Appl. Phys.*, vol. 40, no. 24, pp. 7698–7706, 2007.
[16] H. Rabat and C. de Izarra, "Check of OH rotational temperature using an interferometric method," *J. Phys. D, Appl. Phys.*, vol. 37, no. 17, pp. 2371–2375, 2004.
[17] R. Joussot, D. Hong, H. Rabat, V. Boucinha, R. Weber-Rozenbaum, and A. Leroy-Chesneau, "Thermal characterization of a DBD plasma actuator: Dielectric temperature measurements using infrared thermography," in *Proc. 40th AIAA Fluid Dyn. Conf. and Exhibit.*, Chicago, IL, USA, Jun./Jul. 2010.
[18] V. Boucinha *et al.*, "Characterization of the ionic wind induced by a sine DBD actuator used for laminar-to-turbulent transition delay," in *Proc. 4th Flow Control Conf.*, Seattle, WA, USA, Jun. 2008.
[19] M. Forte, J. Jolibois, J. Pons, E. Moreau, G. Touchard, and M. Cazalens, "Optimization of a dielectric barrier discharge actuator by stationary and non-stationary measurements of the induced flow velocity: Application to airflow control," *Experim. Fluids*, vol. 43, no. 6, pp. 917–928, 2007.

Jérôme Pons received the Ph.D. degree from the University of Orléans, Orléans, France, in 2003, and studied capillary discharge plasmas dedicated to XUV radiation generation.

He was with Old Dominion University, Norfolk, VA, USA, from 2005 to 2006, where he was involved in atmospheric pressure glow discharges. He has been a Post-Doctoral Researcher of DBD Plasma Actuators with the Institut Pprime, University of Poitiers, Poitiers, France, since 2003, and Groupe de Recherches sur l'Energétique des Milieux Ionisés, Université d'Orléans, and PRISME Laboratories, Orléans. He is currently a Professor of Mechanical Engineering with the Institut Universitaire de Technologie, Orléans.

Hervé Rabat received the M.Sc. degree in physics and applications from the University of Limoges, Limoges, France, in 2001, and the Ph.D. degree in gas and plasma physics from the University of Orléans, Orléans, France, in 2004.

He is currently a Research Engineer with the Centre National de la Recherche Scientifique, Groupe de Recherches sur l'Energétique des Milieux Ionisés, University of Orléans.

Annie Leroy received the Ph.D. degree in fluid mechanics from the University of Orléans, Orléans, France, in 1997.

She is currently an Associate Professor with the Institute of Technology and the PRISME Laboratory, University of Orléans. She teaches mainly mechanical engineering and fluid mechanics. She is involved in wind tunnel experiments dedicated to refine physical understanding and characterization of flows, in view of active flow control studies, more specifically with plasma actuators. Her current research interests include aerodynamic flows.

Dunpin Hong (M'10) received the M.Sc. degree from the University of Grenoble, Grenoble, France, and the Ph.D. degree in plasma spectroscopy from the University of Orléans, Orléans, France.

He is currently a Professor with the University of Orléans and the Groupe de Recherches sur l'Energétique des Milieux Ionisés, a Joint Laboratory of the Centre National de la Recherche Scientifique and the University of Orléans. His current research interests include plasma production by electric discharge, optical diagnostics of transient plasmas, and nonthermal plasmas for subsonic airflow control.

Dr. Hong is a member of the French Associations Association des Arcs Electriques and Electronique, Electrotechnique, Automatique.